Acta Biomaterialia 141 (2022) 244–254

Contents lists available at ScienceDirect

Acta Biomaterialia

journal homepage: www.elsevier.com/locate/actbio

Full length article

Biomechanics of mitral valve leaflets: Second harmonic generation microscopy, biaxial mechanical tests and tissue modeling

Mohammad Javad Sadeghinia[a,*], Bjørn Skallerud[a], Gerhard A. Holzapfel[a,b], Victorien Prot[a]

[a] Department of Structural Engineering, Norwegian University of Science and Technology, Trondheim, Norway
[b] Institute of Biomechanics, Graz University of Technology, Austria

ARTICLE INFO

Article history:
Received 19 October 2021
Revised 10 December 2021
Accepted 3 January 2022
Available online 8 January 2022

Keywords:
Mitral valve leaflet
Collagen fiber
Second harmonic generation microscopy
Planar biaxial mechanical test
Tissue model

ABSTRACT

Collagen fibers are the main load carrier in the mitral valve (MV) leaflets. Their orientation and dispersion are an important factor for the mechanical behavior. Most recent studies of collagen fibers in MVs lack either entire thickness study or high transmural resolution. The present study uses second harmonic generation (SHG) microscopy in combination with planar biaxial mechanical tests to better model and examine collagen fibers and mechanical properties of MV leaflets. SHG in combination with tissue clearing enables the collagen fibers to be examined through the entire thickness of the MV leaflets. Planar biaxial mechanical tests, on the other hand, enable the characterization of the mechanical tissue behavior, which is represented by a structural tissue model. Twelve porcine MV leaflets are examined. The SHG recording shows that the mean fiber angle for all samples varies on average by $\pm 12^{\circ}$ over the entire thickness and the collagen fiber dispersion changes strongly over the thickness. A constitutive model based on the generalized structure tensor approach is used for the associated tissue characterization. The model represents the tissue with three mechanical parameters plus the mean fiber direction and the dispersion, and predicts the biomechanical response of the leaflets with a good agreement (average $r^2 = 0.94$). It is found that the collagen structure can be represented by a mean direction and a dispersion with a single family of fibers despite the variation in the collagen fiber direction and the dispersion over the entire thickness of MV leaflets.

Statement of significance

Despite its prominent role in the mechanical behavior of mitral valve (MV) leaflets, the collagen structure has not yet been investigated over the entire thickness with high transmural resolution. The present study quantifies the detailed through thickness collagen fiber structure and examines the effects of its variation on MV tissue modeling. This is important because the study evaluates the assumption that the collagen fibers can be modeled with a representative single fiber family despite the variation across the thickness. In addition, the current comprehensive data set paves the way for quantifying the disruption of collagen fibers in myxomatous MV leaflets associated with disrupted collagen fibers.

1. Introduction

The mitral valve (MV) ensures the unidirectional flow from the left atrium to the left ventricle. The unique microstructure of the MV leaflets enables very high stretch rates, as reported in, e.g., [1]. This makes it easier to close the valve completely during systole. The MV leaflet consists of four different layers: an elastic ventricularis, a collagen-rich fibrosa, a spongiosa layer consists of mostly proteoglycans and an elastic atrialis. Collagen acts as the main load carrier, while elastin, which is also found in all other layers, restores the wavy state of the collagen fibers [2].

Numerous diseases associated with MV, such as myxomatous degeneration, disrupt the microstructure of the leaflets and contribute to partial closure and thus to MV regurgitation [3], which is defined as the leakage of blood from the left ventricle into the left atrium, with severe cases requiring careful assessment [4]. In particular, the collagen fibers were observed as disrupted and irreg-

* Corresponding author.
E-mail address: mj.sadeghinia@ntnu.no (M.J. Sadeghinia).

https://doi.org/10.1016/j.actbio.2022.01.003

ularly arranged in the accompanying diseases [5,6]. Barlow's disease, e.g., is associated with disrupted collagen fibers and increased leaflet compliance [3]. Therefore, a precise mechanical characterization of the MV leaflets, whether healthy or diseased, requires a detailed investigation of the collagen fiber dispersion.

Various imaging methods were used for the identification of the collagen fiber dispersion: polarized spatial frequency domain imaging (pFSDI) [7,8], small-angle light or X-ray scattering (SALS or SAXS) [9,10] and second harmonic generation (SHG) [11,12]; for a short overview see [13]. SHG provides collagen imaging of the sample with high transmural resolution that enables a detailed in-depth study of the collagen structure. To the best of the authors' knowledge, there are only two studies on the collagen fiber structure in MV leaflets with SHG [11,14]. The study [14] used *'representative SHG images to visualize local fiber architecture'* without quantification. The study [11] quantified the fiber distribution of an ovine sample, which was taken from both sides up to a thickness of 100 μm in order to include all layers of the MV leaflets. Nonetheless, the limited depth of SHG acquisition may have missed most of the fibrosa layer, the collagen-rich layer in MV leaflets. In order to overcome this limitation, the imaging depth can be increased up to 1 000 μm, by using tissue clearing methods as proposed in the study [12] for arteries.

The quantified collagen fiber distribution can then be used in addition to mechanical tests to characterize the tissues of the MV leaflets. Several recent studies used planar biaxial mechanical tests with various imaging methods to characterize the tissue properties of MV leaflets [8,14–16]. Nonetheless, either aggregated or limited in-depth SHG imaging was used in these studies. A very recent study [17] used SHG with tissue clearing for mechanical and microstructural analysis of the tricuspid valve in ovine without tissue modeling. Therefore, there is a lack of comprehensive information on how the dispersion and orientation of collagen fibers vary across the thickness of the MV leaflets and between different samples. More importantly, the effects of this variation on tissue modeling of MV leaflets have yet to be explored. The variation of the collagen fiber dispersion and orientation can, e.g., indicate whether it is sufficient to use a representative distribution or whether a layered approach is required. In addition, a comprehensive data set paves the way for quantifying the disruption of collagen fibers in diseased MV leaflets.

The present study uses planar biaxial mechanical tests in combination with SHG to characterize twelve MV leaflets. Porcine samples are used since they are anatomically similar to healthy human MVs [18]. First, the samples are examined with a custom-built planar biaxial machine. They are then chemically fixed and cleared for SHG imaging, which is carried out across the entire thickness of the samples. The collagen fiber dispersions and orientations are quantified using image analysis [12]. In order to represent the tissue behavior of the samples, a constitutive model based on the generalized structure tensor approach is used [19]. In addition to the mean fiber direction and the in-plane dispersion of collagen fibers, which are quantified by SHG, the model uses three mechanical parameters estimated from the planar biaxial mechanical tests to characterize the tissue properties of MV leaflets.

2. Materials and methods

2.1. Tissue acquisition and storage

In this study, six MV anterior leaflets (MVAL) and six posterior leaflets (MVPL) are examined. They are cut from 7 fresh porcine hearts (P1-P7) from Nortura slaughterhouse in Steinkjer, Norway (the MVPL sample from P6 and the MVAL sample from P7 could not be used). The hearts are kept at refrigerator temperature during transport. After the excision, the leaflets are labeled and stored in freezers at −28°C before testing.

2.2. Planar biaxial testing

To prepare the sample for the test, it is first thawed at 4° and then at room temperature in a 1×PBS solution. The sample is then cut apart (Fig. 1(a)), and its anatomical direction is identified and marked with three indicative markers on the upper right of the sample (Fig. 1(b)), using tissue marking dye (Leica Biosystems, Germany). The circumferential direction is assumed to be approximately parallel to the mitral annulus. The sample thickness is then measured three times with a caliper (0.01mm resolution), whereby the average value is reported. Finally, it is attached to four barbless hooks (Ahrex, Denmark) on each side, using a 3D printed template for consistency. This provides an effective test area of 10 mm ×10 mm. The sample is additionally marked with four fiducial markers in the center, with an approximate area of 2 mm ×2 mm, as shown in Fig. 1(b).

The hooks are connected to the handle mechanism with surgical Gore-Tex CV5 sutures (Gore Medicals, USA). The custom-designed handle mechanism, shown in Fig. 1(c), consists of a rotatable base with two 1 mm thick bars that represent the attachment sites for the sutures. These bars can rotate freely around the base axis, which is equipped with an all-ceramic bearing (SMB Bearings, UK). This mechanism enables self-alignment when mounting the specimen and minimizes the shear forces during the experiments.

The custom-built biaxial machine is equipped with four step motors that are individually controlled via an inductive displacement sensor (BAW M18MG, Balluff, Germany). The loads are also measured with an axial load transducer (U9C/50 HBM, Germany). Using a custom software for digital image correlation [20], the position of the fiducial markers is tracked during the test and synchronized with the measured forces at a frequency of 2 Hz. The biaxial machine was validated using a rubber-like material and compared to a commercial uniaxial machine (Instron, USA).

Before starting the test, a preconditioning of 5 loading-unloading cycles at a rate of 0.1 mm/s is applied to the maximum load of 0.85 ± 0.15 N. The sample is also subjected to a preload of 0.01 N in both directions to remove any tissue slack. Two series of displacement-controlled tests, each repeated three times, are carried out at a speed of 0.1 mm/s up to the maximum load of 0.85 ± 0.15 N; one with a 1 : 1 displacement in the circumferential and radial direction and the other with a greater displacement in the radial direction. During the entire test, the sample is submerged in a 1×PBS solution at 37°C.

2.3. Tissue fixation, dehydration and tissue clearing

Chemical fixation occurs within 2 hours of thawing. Samples are chemically fixed in a 4% formaldehyde solution for a minimum of 36 hours and also dehydrated based on graded absolute ethanol: 50%, twice 70%, twice 95% and twice 100%, each step lasts 30 min [12]. The fixation and dehydration take place in an automated vacuum tissue processor (ASP 300, Leica Biosystems, Germany). The fixed and dehydrated sample is shown in Fig. 2(a).

After fixation and dehydration, the sample is cleared with 1 : 2 benzyl alcohol : benzyl benzoate (BABB) as a clearing solvent. This technique was introduced in [21] and adopted for biomechanical application in the studies [22,23]. The tissue is first immersed in 1 : 1 absolute ethanol : BABB solution for 4 hours and then in BABB solution for 18 hours. A representative cleared sample is shown in Fig. 2(b), the same as in Fig. 2(a). After the tissue has been cleared, the sample is placed in a bottom-glass dish with a few drops of BABB solution and sealed with a cover glass using CoverGrip sealant (Biotium Inc., USA).

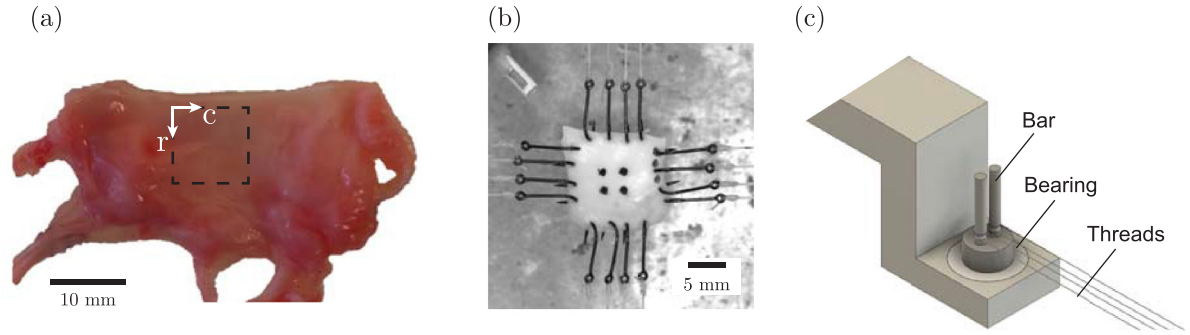

Fig. 1. Sample preparation and mounting on the biaxial machine: (a) preparation of the MV leaflets (r = radial, c = circumferential) (b) hooks attachment to the samples, four fiducial markers in the center and three indicative markers on the upper right of the sample; (c) handle mechanism equipped with a bearing that enables self-alignment and ensures that shear forces are minimized during the experiment.

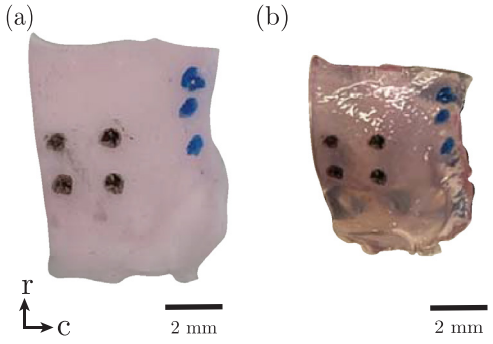

Fig. 2. Sample preparation for SHG microscopy: (a) chemically fixed and dehydrated sample (b) chemically cleared sample for SHG imaging showing the same sample as in (a).

2.4. Second harmonic generation microscopy

SHG imaging of collagen fibers is performed using a Leica SP8 confocal microscope (Leica Microsystem, Germany). Before the SHG acquisition, the measurement of the entire thickness is verified with the bright field microscope in the Leica SP8 to ensure that the SHG scanning occurs through the entire thickness of the samples. To induce the second harmonic of a collagen fiber, the laser excitation is set to 890 nm. The Leica HCX IRAPO 25×, NA 0.95 water objective with a working distance of 2.4 mm is used for image acquisition. To compensate for scattering at greater depth, the laser power is increased linearly (z compensation). The scanning takes place in the center of the fiducial markers with an area of 465 μm ×465 μm and a resolution of 0.45 μm/pixel from the ventricular side. The imaging over the entire tissue thickness takes place with an interval of 5 μm. Fig. 3(a) shows a representative SHG acquisition layer for sample P3-MVPL at a depth of 200 μm from the ventricular side.

A user-defined MATLAB [24] script based on the method documented in [12] is used to quantify the collagen fiber dispersion in each layer. Before the analysis, a 2D Tukey (tapered cosine) window is applied to the image. Each image is then Fourier transformed and multiplied by its conjugate complex to form the power spectrum density, which distinguishes the fiber direction by frequency and orientation. A wedge-shape filter is used to extract the fiber orientations at a certain angle θ. The wedge-shape filter ranges from −89° to 90° with an increment of 1° to determine the relative amplitude of the fiber distribution, for a representative result see Fig. 3(b). A moving average filter with a range of 7° is then applied to the angle θ to smooth the data. Multiple anisotropic layers are found, as they are described in [12] as anisotropic fiber distribution, see Fig. 1 therein. For a certain anisotropic layer, labeled as l, the fiber distribution is then fitted by a von Mises distribution, which is defined as

$$\rho^l(\theta) = \sum_{m=1}^{n^l} \frac{\exp\{a_m^l \cos[2(\theta - \alpha_m^l)]\}}{I_0(a_m^l)}, \quad -90^\circ < \alpha_m^l \le 90^\circ, \quad 1 \le l \le L. \tag{1}$$

Herein $\rho^l(\theta)$ is the von Mises distribution in layer l characterized byn^l, the number of fiber families, while α_m^l denotes the mean fiber angle of the fiber family m, $a_m^l > 0$ is the concentration parameter for the fiber family m, L is the total number of layers across the thickness, and I_0 denotes the modified Bessel function of order zero. A sample with L acquisition layers is represented by average values, which we denote by a bar on the respective value, e.g., $\bar{a}$ for the averaged concentration parameter. Note that a higher value of $\bar{a}$ means a higher anisotropy of the tissue. The fiber angles α_m^l are orientation data with values $-90^\circ < \alpha_m^l \le 90^\circ$, thus averaged accordingly [25]. In addition to the collagen fiber distribution, the collagen fiber content in each layer is examined by the skewness of the pixel intensity histogram. A study on celluralized collagen gels showed that skewness, a gain-independent parameter, correlates inversely with the collagen content [26]. The skewness S is defined as

$$S = \frac{n}{(n-1)(n-2)} \sum_{i=1}^{n} \frac{(x_i - \bar{x})^3}{s^3}, \tag{2}$$

where x_i is the pixel intensity, n is the number of pixels in each image, $\bar{x}$ and s are the mean and standard deviation of the pixel intensities, respectively. In the current study, the image histogram and its respective skewness are calculated using MATLAB [24].

2.5. Tissue model

The deformation gradient $\mathbf{F}$ is defined in relation to an undeformed reference configuration that is assumed to be stress-free. The right Cauchy-Green tensor is then calculated as $\mathbf{C} = \mathbf{F}^{\mathrm{T}}\mathbf{F}$ [27]. A constitutive model based on the generalized structure tensor approach with non-symmetric collagen fiber dispersion is chosen [19]. The strain–energy function Ψ is decoupled into an isotropic part Ψ_{iso} and an anisotropic (fiber) part Ψ_{fib}. The isotropic function is assumed as the neoHookean model, i.e.

$$\Psi_{\mathrm{iso}} = \frac{\mu}{2}(I_1 - 3), \qquad I_1 = \mathrm{tr}\mathbf{C}, \tag{3}$$

where $\mu > 0$ is a positive material parameter and I_1 is the first invariant of $\mathbf{C}$, where tr(•) denotes the trace of (•). The fiber function is assumed to be [19]

$$\Psi_{\mathrm{fib}} = \frac{k_1}{2k_2}\{\exp[k_2(I_4^* - 1)^2] - 1\}, \qquad I_4^* = \mathrm{tr}(\mathbf{CH}), \tag{4}$$

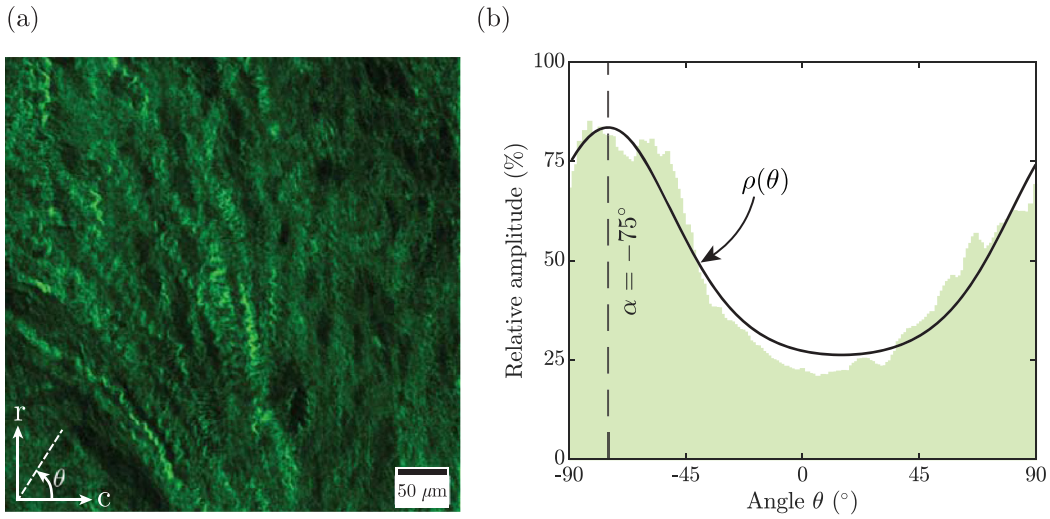

Fig. 3. SHG imaging and analysis of collagen fibers for sample P3-MVPL: (a) SHG acquisition at a depth of 25% from the ventricular side (green = collagen, r = radial, c = circumferential); (b) corresponding relative amplitude of the collagen fibers (green area) and fitted von Mises distribution (solid curve) with $\theta = 0^\circ$ corresponding to the circumferential direction. The von Mises parameters are $\alpha = -75^\circ$, $a = 1.18$, with $r^2 = 0.94$. (For interpretation of the references to colour in this figure legend, the reader is referred to the web version of this article.)

where k_1 and k_2 are positive material parameters and $\mathbf{H}$ is the structure tensor [19,28], i.e.

$$\mathbf{H} = 2\kappa_{op}\kappa_{ip}\mathbf{I} + 2\kappa_{op}\big(1-2\kappa_{ip}\big)\mathbf{M}\otimes\mathbf{M} + \big(1-2\kappa_{op}-2\kappa_{op}\kappa_{ip}\big)\mathbf{M}_n\otimes\mathbf{M}_n. \tag{5}$$

Herein $\mathbf{I}$ is the second-order identity tensor, $\mathbf{M}$ and $\mathbf{M}_n$ are the mean fiber direction and the out-of-plane unit vector in the reference configuration, respectively, while κ_{ip} and κ_{op} are the in-plane and out-of-plane dispersion parameters. If the tissue is assumed to be incompressible the (total) strain–energy function Ψ can then be defined as

$$\Psi = \Psi_{iso} + \Psi_{fib} + p(J-1), \quad J = \det\mathbf{F} > 0, \tag{6}$$

where p is a Lagrange multiplier used to enforce incompressibility, and J is the positive volume ratio.

Now we define three orthogonal unit vectors as $\mathbf{e}_c$, $\mathbf{e}_r$ and $\mathbf{e}_t$, which denote the circumferential, radial and transmural directions, respectively. In this coordinate system, the deformation gradient $\mathbf{F}$ is calculated from the fiducial markers, as explained in, e.g., [29]. The off-diagonal components of the $\mathbf{C}$ matrix are at least an order of magnitude smaller that the diagonal components. So it is assumed that the matrix $\mathbf{C}$ only adds diagonal components, namely the squares of the principal stretches λ_c^2, λ_r^2 and λ_t^2. Because of incompressibility, the principal stretch λ_t through the thickness is $(\lambda_c\lambda_r)^{-1}$. The mean fiber direction $\mathbf{M}$ related to the circumferential direction is given by $\mathbf{M} = \cos\alpha\,\mathbf{e}_c + \sin\alpha\,\mathbf{e}_r$. The push forward of the structure tensor $\mathbf{H}$ results in $\mathbf{h} = \mathbf{F}\mathbf{H}\mathbf{F}^T$, so that the modified fourth invariant $(4)_2$ can be calculated as [19]

$$I_4^* = \mathrm{tr}(\mathbf{C}\mathbf{H}) = \mathrm{tr}\mathbf{h} = h_{11} + h_{22} + h_{33}, \tag{7}$$

with the diagonal components of $\mathbf{h}$ according to

$$\begin{aligned} h_{11} &= 2\kappa_{op}\big[\kappa_{ip} + \big(1-2\kappa_{ip}\big)\cos^2\alpha\big]\lambda_c^2,\\ h_{22} &= 2\kappa_{op}\big[\kappa_{ip} + \big(1-2\kappa_{ip}\big)\sin^2\alpha\big]\lambda_r^2,\\ h_{33} &= (1-2\kappa_{op})\lambda_t^2. \end{aligned} \tag{8}$$

The collagen structure in mitral valves is assumed to be planar, so we use the upper limit of κ_{op} which equals 1/2, so that $h_{33} = 0$. This leads to a reduced 2×2 matrix of $\mathbf{h}$, which is a planar dispersion. Now, κ_{ip} can be related to $\bar{a}$, which is the averaged concentration parameter of all layers, so that

$$\kappa_{ip} = \frac{1}{2} - \frac{I_1(\bar{a})}{2I_0(\bar{a})}, \qquad 0 \le \kappa_{ip} < 1/2, \tag{9}$$

where I_0 is the Bessel function of the first kind of order 0, while I_1 is the modified Bessel function of the first kind of order 1. Note that $\kappa_{ip} = 1/2$ corresponds to a planar isotropic dispersion and the lower κ_{ip}, the higher the anisotropy. Finally, the non-zero Cauchy stress components are

$$\sigma_{cc} = \mu\big(\lambda_c^2 - \lambda_t^2\big) + 4k_1\big(I_4^{*2}-1\big)\exp\Big[k_2\big(I_4^{*2}-1\big)^2\Big]h_{11}, \tag{10}$$

$$\sigma_{rr} = \mu\big(\lambda_r^2 - \lambda_t^2\big) + 4k_1\big(I_4^{*2}-1\big)\exp\Big[k_2\big(I_4^{*2}-1\big)^2\Big]h_{22}, \tag{11}$$

with

$$\begin{aligned} h_{11} &= \big[\kappa_{ip} + \big(1-2\kappa_{ip}\big)\cos^2\alpha\big]\lambda_c^2,\\ h_{22} &= \big[\kappa_{ip} + \big(1-2\kappa_{ip}\big)\sin^2\alpha\big]\lambda_r^2,\\ I_4^* &= h_{11} + h_{22}. \end{aligned} \tag{12}$$

The stresses σ_{cc} and σ_{rr} are calculated from the measured forces, thickness, the effective area measured between the hooks, as suggested in [30], and the calculated deformation gradient. The mean fiber angle and the in-plane dispersion parameter are obtained from the SHG images, as described in Section 2.4. The parameters μ, k_1, k_2 are found with a nonlinear least squares methods (trust region reflective algorithm), implemented in MATLAB [24], from planar biaxial mechanical tests. It is assumed that the initial values are the same for all samples with values of 1.0 kPa, 2.0 kPa and 10.0, respectively. Some other starting values are also tested to ensure that the fitted parameters do not correspond to the local minimum.

3. Results

The solvent-based clearing with BABB made it possible to record the entire thickness of the samples with SHG. The acquisition depth before clearing was limited to 100 μm [31]. After tissue

clearing, the samples were scanned to a depth of 700 μm. However, this solvent-based clearing usually have a shrinkage effect [31], which can also be seen in Fig. 2. Similar to the previously reported studies [12,32,33], the shrinkage of the sample was found to be about isotropic without any interference with the collagen dispersion in the plane of acquisition. In the present work, a shrinkage of 23% and 20% in the respective radial and circumferential direction was measured for the sample shown in Fig. 2, using the fiducial markers.

Fig. 4 shows the collagen fiber distributions in the form of contour plots for all samples. Therein the relative amplitude of collagen fiber, which is oriented at a certain angle θ (abscissa) and at a certain depth (ordinate), is indicated by the color map. For example, the distribution of collagen fiber shown in Fig. 3 is the same as the contour plot at the depth of 25% for sample P3-MVPL. As shown in Fig. 4, most samples are collagen-rich with a thickness of 0 – 50%, corresponding to the collagen-rich fibrosa layer [2]. For one anterior sample (P3-MVAL), the collagen fiber distribution in most layers shows two different fiber orientations. For example, at the same depth of 80% for this sample, two bright spots are observed in Fig. 4; one oriented at a positive angle and the other, with less relative amplitude, oriented at a negative angle. The SHG imaging and analysis of collagen fibers for this sample at the same depth is shown in Fig. 5. The same result can also be observed with two distinct peaks in Fig. 5(b); one oriented at 15° and the other, with a lower relative amplitude, oriented at −54°. Only for this sample two fiber families are assumed ($m = 2$, based on Eq. (1)) for the fitting of the von Mises distribution function to the fiber distribution in each layer. For reasons of consistency, the concentration parameter and the mean fiber angle, which correspond to the fiber families with higher relative amplitudes, were used to calculate the averaged values of $\bar{a}$ and $\bar{\alpha}$. For all other samples only one fiber family ($m = 1$) is assumed for all layers, as shown in Fig. 3(b).

The corresponding von Mises parameters for the 12 samples and related statistics are presented in Table 1 with a 10% thickness interval including only anisotropic layers, as defined in Section 2.4.

The average values for the mean fiber angle $\bar{\alpha}$ and the concentration parameter $\bar{a}$ are calculated based on all anisotropic layers between 0 – 100% thickness. The positive and negative mean angles between the samples can be explained by the different test locations on the MV leaflets, as shown in Fig. 6. The mean direction is positive when the sample is taken from the right side of the approximate symmetry axis and negative when it is taken from the left side of the axis. In numerous samples, the standard deviation of the mean fiber angle $\bar{\alpha}$ is rather small. However, it was found that one anterior leaflet (P2-MVAL) had two perpendicular mean fiber orientations across its thickness, therefore the mean fiber orientation changes from the ventricular to the atrial side by about 90°. One is oriented in the circumferential direction from 0 – 60% depth and the other is oriented almost in the radial direction from 60 – 100% depth.

After all, the mean fiber direction is not always aligned with the circumferential direction, as shown in the Fig.s 3 and 4. It is worth mentioning that the fiber directions are given for $-90^\circ < \theta \leq 90^\circ$, but they are orientation data. In other words, e.g., −60° also corresponds to 120°. The standard deviation of the fiber angles over the entire thickness is, on average over the samples, 12°. Even for the sample P3-MVAL, which has two distinct fibers, the mean orientation for the more pronounced fiber family varied with a standard deviation of 11° over the entire tissue thickness. The variation of the dispersion parameter is more pronounced than the fiber directions. Sample P2-MVAL also exhibited an exceptionally high anisotropy in the thickness of 20 – 60% with a $\bar{a}$ value of more than 15. This is also noticeable in Fig. 4. Nonetheless, the average concentration parameter $\bar{a}$ was found to be 1.16 ± 0.32 for all

Table 1
Average values for the mean fiber angle $\bar{\alpha}$ and the concentration parameter $\bar{a}$ from the von Mises distribution for 12 samples, six MV anterior leaflets (MVAL) and six posterior leaflets (MVPL) from 7 porcine hearts (P1-P7). Parameters are given for 10% thickness intervals. Depths with no anisotropic layers are intentionally left out. The last rows indicate the average, the standard deviation (STD), and the average r^2 for the samples. Note that the fiber angles $\bar{\alpha}$ are orientation data (i.e. −60° also corresponds to 120°), thus averaged accordingly [25].

Sample	P1-MVAL		P1-MVPL		P2-MVAL		P2-MVPL		P3-MVAL		P3-MVPL		P4-MVAL		P4-MVPL		P5-MVAL		P5-MVPL		P6-MVAL		P7-MVPL	
Thickness	$\bar{\alpha}$(°)	$\bar{a}$(–)	$\bar{\alpha}$(°)	$\bar{a}$(–)	$\bar{\alpha}$(°)	$\bar{a}$(–)	$\bar{\alpha}$(°)	$\bar{a}$(–)	$\bar{\alpha}$(°)	$\bar{a}$(–)	$\bar{\alpha}$(°)	$\bar{a}$(–)	$\bar{\alpha}$(°)	$\bar{a}$(–)	$\bar{\alpha}$(°)	$\bar{a}$(–)	$\bar{\alpha}$(°)	$\bar{a}$(–)	$\bar{\alpha}$(°)	$\bar{a}$(–)	$\bar{\alpha}$(°)	$\bar{a}$(–)	$\bar{\alpha}$(°)	$\bar{a}$(–)
0-10%	12	1.09	−66	0.86	−30	2.07	55	1.74	35	0.63	−77	1.26	21	0.67	−15	2.97	−4	1.25	9	1.25	51	0.87	−44	0.96
10-20%	19	1.36	−68	0.91					36	0.6	−76	1.35	−4	0.66	−12	2.08	−11	1.27	7	1.06	65	1.17	−35	1.1
20-30%	3	1.06	−67	0.89	−4	13.09			31	0.83	−75	1.19	−35	1.68	−16	2.06	−11	0.88	−8	0.91	72	1.33		
30-40%	−2	1.31	−65	0.98	−1	19.23			32	1.02	−68	1.17	−41	1.86	−15	1.63	−13	0.48	−11	1.12	79	1.56		
40-50%	−2	1.36			−2	33.07			33	0.85	−66	1.68	−56	2.55	−23	1.18	3	0.47	−8	1.17	88	1.48		
50-60%	−2	1.14	−73	0.7	−46	14.04			33	0.77	−67	1.3	−57	2.17	−25	1	−5	0.7	−5	1.15	−88	0.99		
60-70%	−7	0.9	−72	0.73	86	15.21			28	0.37	−66	1.22	−60	2.28	−22	0.86	−5	1	−6	1.22	79	0.44		
70-80%	9	0.7			86	2			34	0.79	−68	1.06	−61	2	−21	0.93	−7	1.02	−6	1.09	0	0		
80-90%	9	0.54			81	1.55			19	0.72	−72	1.05	−66	1.54	−29	0.88	10	0.74	−2	0.99	−75	0.55		
90-100%	0	0							34	0.76	−78	0.97					45	0.53	−12	0.81	−71	0.66		
Average	3	1.09	−68	0.86	−13	12.57	55	1.7	32	0.74	−71	1.22	−47	1.71	−19	1.47	−2	0.83	−4	1.07	81	1.05	−40	1.02
STD	9	0.31	3	0.11	36	12.98	2	0.21	11	0.23	6	0.3	25	0.68	6	0.64	15	0.31	8	0.17	18	0.39	4	0.07
Average r^2	0.85		0.87		0.89		0.95		0.9		0.87		0.91		0.93		0.83		0.9		0.89		0.92	

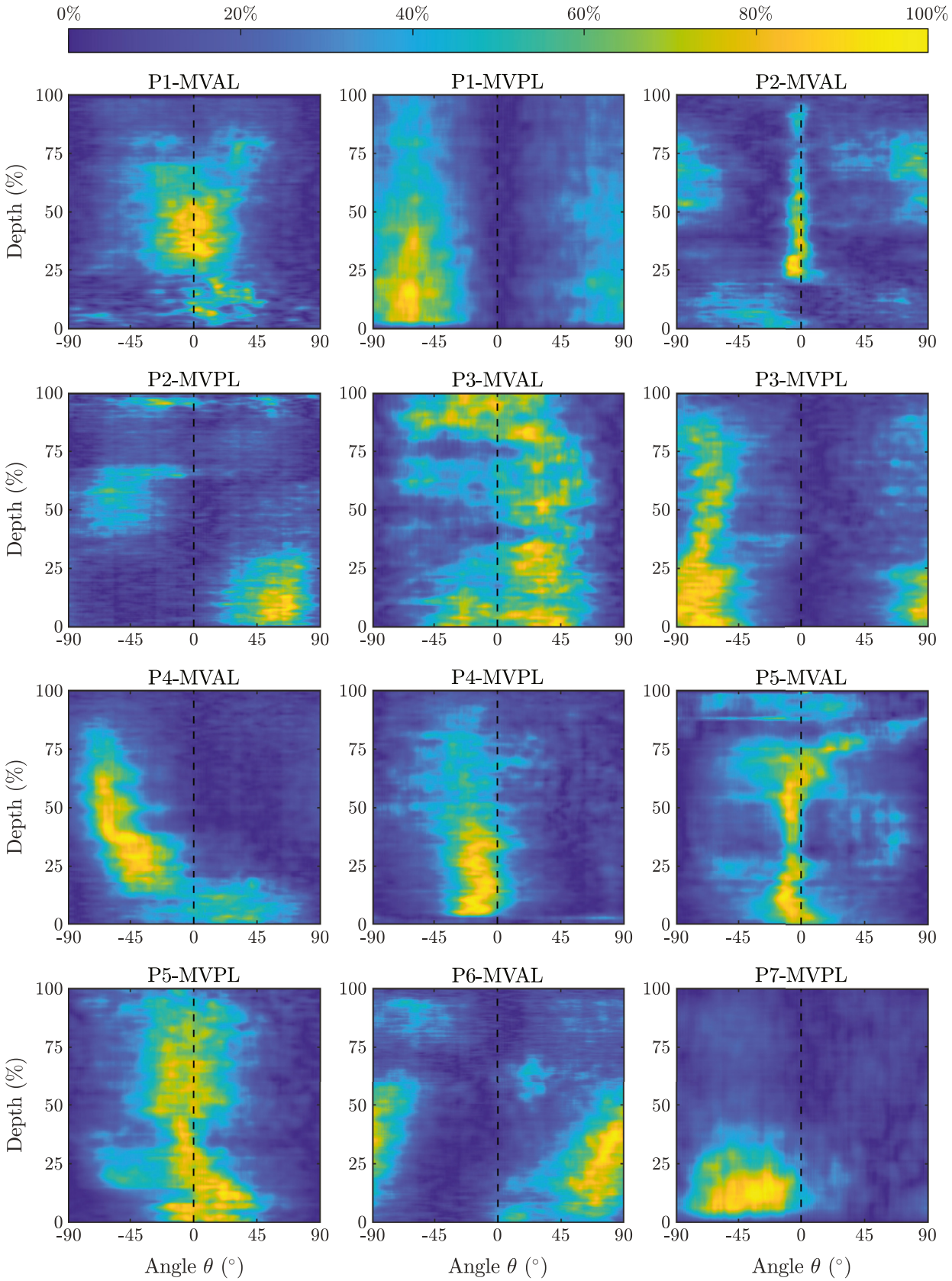

Fig. 4. Relative amplitude of collagen fibers across the entire thickness for the 7 porcine hearts (P1-P7) displaying six MV anterior leaflets (MVAL) and six posterior leaflets (MVPL): The circumferential direction and ventricular side correspond to $\theta = 0^{\circ}$ and 0% depth, respectively.

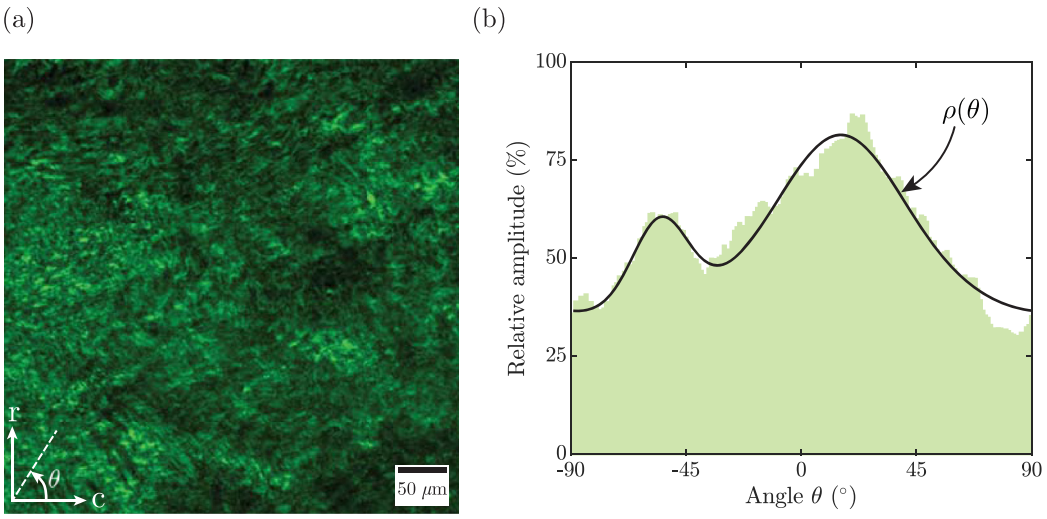

Fig. 5. Two fiber families are identified for sample P3-MVAL ($m = 2$): (a) SHG acquisition at a depth of 80% from the ventricular side (green = collagen, r = radial, c = circumferential); (b) relative amplitude of the collagen fibers (green area) and fitted von Mises distribution (solid curve). The von Mises parameters are $\alpha_1 = 15^\circ$, $a_1 = 1.13$ and $\alpha_2 = -54^\circ$, $a_2 = 6.68$, with $r^2 = 0.94$. The more pronounced fiber family (oriented at $\alpha_1 = 15^\circ$) was used for further post-processing. (For interpretation of the references to colour in this figure legend, the reader is referred to the web version of this article.)

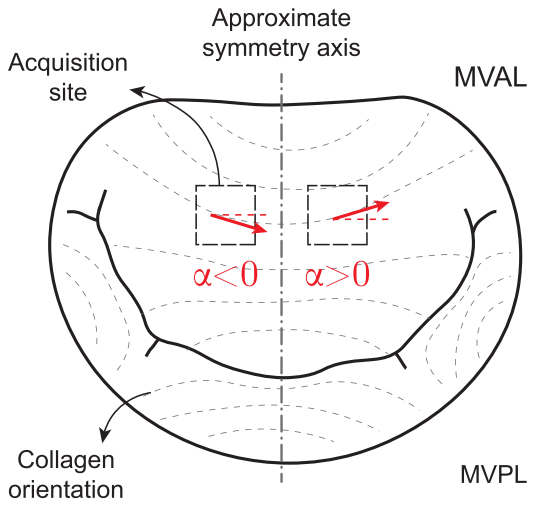

Fig. 6. General collagen fiber distribution (dashed curves) over the mitral valve leaflets, composed of MVAL (MV anterior leaflet) and MVPL (MV posterior leaflet), with an approximate axis of symmetry (dashed and dotted line). The sign of the mean fiber angle α depends on the acquisition site (dashed squares).

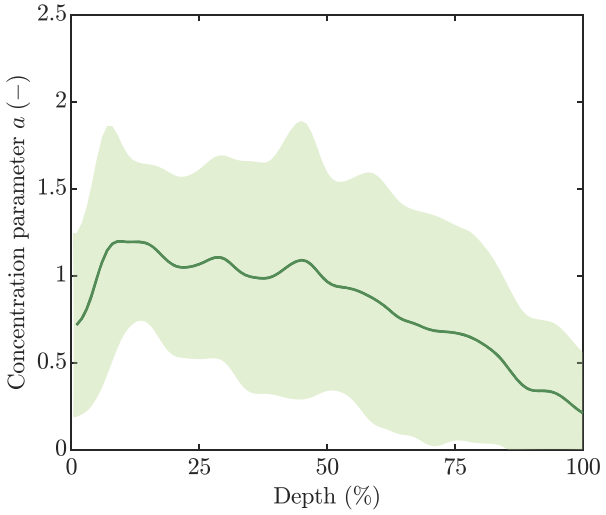

Fig. 7. Variation of the concentration parameter a through the normalized thickness; averaged value between the samples, with the exception of sample P2-MVAL (solid curve) and standard deviation (colored area).

samples excluding P2-MVAL. Fig. 7 shows the variation of the concentration parameter a through the normalized thickness, averaged between all samples except P2-MVAL, which showed an exceptionally high anisotropy. It was found that the samples had, on average, a higher anisotropy at a depth of $5 - 50\%$, which corresponds to the collagen-rich fibrosa layer in MV. The concentration of the collagen content is also investigated using the skewness of the image (layer) histogram. The variation in skewness between samples due to the normalized thickness is shown in Fig. 8. According to the study of [26], the collagen content correlates inversely with the skewness. Therefore, collagen fibers are more pronounced at a depth of $25 - 75\%$. The constitutive model predicts the mechanical behavior of the leaflets with good agreement (average r^2-value is 0.94). This is shown for two samples in Fig. 9, one sample with the circumferentially oriented collagen fibers (Fig. 9(a)) and the other with radially oriented collagen fibers (Fig. 9(b)). The data for the characterized material and structural parameters are presented in Table 2. The neoHookean parameters are relatively small ($\mu = 2.22 \pm 1.48$ kPa). For P1, P4 and P3, the neoHookean param-

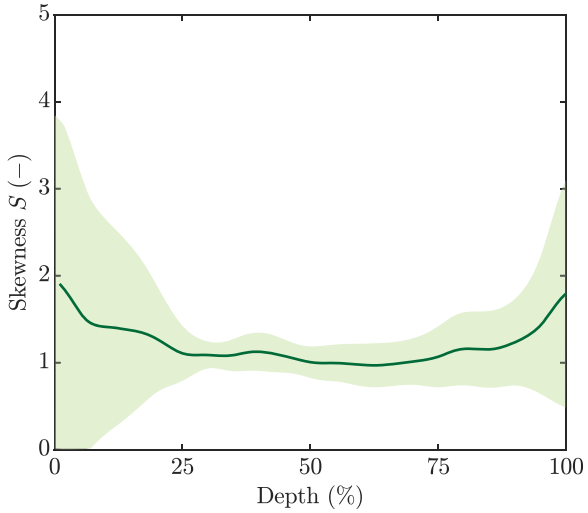

Fig. 8. Variation of the skewness through the normalized thickness; averaged value between the samples (solid curve) and the standard deviation (colored area).

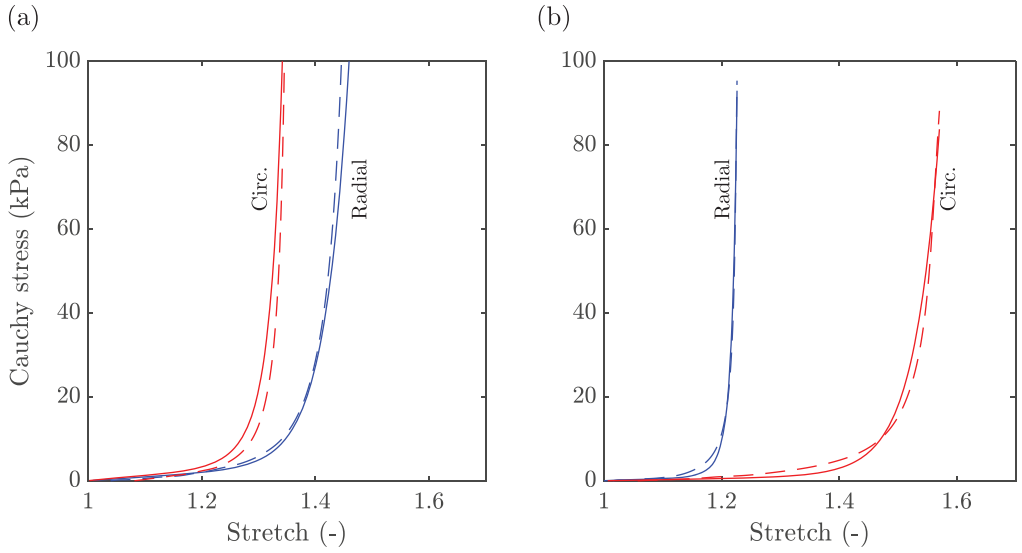

Fig. 9. Cauchy stress σ versus stretch λ for (a) sample P3-MVAL and (b) sample P6-MVAL in the radial (blue curve) and circumferential direction (red curve). The experimental data (dashed curve) are well represented by the model (solid curve) with r^2 of 0.93 (P3-MVAL) and 0.98 (P6-MVAL). (For interpretation of the references to colour in this figure legend, the reader is referred to the web version of this article.)

Table 2
Estimated material parameters from planar biaxial mechanical tests, structural parameters from SHG and thickness t from histology sections. The last column gives the average r^2.

	Planar biaxial data			SHG data				
Parameter	μ(kPa)	k_1(kPa)	$k_2(-)$	$\bar{\alpha}(^\circ)$	$\kappa_{ip}(-)$	$\bar{a}(-)$	t(mm)	r^2
P1-MVAL	1.54	6.04	3.17	3	0.26	1.09	0.85	0.94
P1-MVPL	1.21	1.91	7.65	−68	0.3	0.86	1.45	0.91
P2-MVAL	1.3	0.28	11.37	−13	0.02	12.57	1	0.94
P2-MVPL	3.92	0.87	7.44	55	0.18	1.7	1.05	0.94
P3-MVAL	1.53	0.4	5.4	32	0.33	0.74	1.15	0.93
P3-MVPL	6.16	0.19	13.51	−71	0.24	1.22	1	0.94
P4-MVAL	3.44	8.23	0.71	−47	0.18	1.71	1.05	0.92
P4-MVPL	2.82	3.23	2.34	−19	0.21	1.47	1.05	0.96
P5-MVAL	1.75	2.54	3.87	−2	0.31	0.83	1.05	0.84
P5-MVPL	1.47	1.42	11.72	−4	0.26	1.07	1.2	0.99
P6-MVAL	1.06	0.1	10.76	81	0.27	1.05	1.4	0.98
P7-MVPL	0.44	0.3	8.37	−40	0.27	1.02	0.95	0.96
Average	2.22	2.13	7.19	−19	0.24	2.11	1.1	0.94
STD	1.48	2.38	3.81	35	0.08	3.04	0.16	0.04

eters for the anterior and posterior leaflets are similar. The fiber parameters (k_1 and k_2) for all samples are 2.13 ± 2.38 kPa and 7.19 ± 3.81, respectively.

4. Discussion

Mitral valve leaflets are collagen-reinforced tissues. The orientation and dispersion of the collagen fibers thus have a significant effect on the mechanical behavior of the leaflets. This is particularly important in Barlow's disease, which is accompanied by disrupted collagen fibers and increased leaflet compliance [3]. In the present study, the collagen fiber distribution over the entire thickness of porcine samples was examined using SHG microscopy. Other techniques such as pFSDI, SALS or SAXS examine an aggregated image, which means that all collagen fibers over the entire thickness of the tissue are aggregated in one acquisition plane. The aggregated image can also be disturbed by other MV leaflet components, as was stated in the recent paper [8]. SHG, on the other hand, provides full-thickness collagen imaging of the sample with high transmural resolution, albeit in a smaller field of view, typically hundreds of microns. Even the depth-modulated pFSDI, which was presented in [8], lacks the high transmural resolution of SHG microscopy, which is normally between $0.5 - 1\,\mu$m/pixel.

This study is the first to provide the collagen distribution across the entire thickness of porcine MV leaflets based on SHG. It adapted a solvent-based clearing technique [21] to enable detailed imaging of the samples in the entire thickness. Before clearing, the samples are fixed chemically with formalin in order to preserve the microstructure. A study on the effects of tissue fixation concluded that formalin fixation for 48 hours based on SAXS measurements had little effect on collagen organization [34]. Another study on arteries with a similar tissue clearing protocol confirms that the collagen fibers are intact, based on histological examinations [12]. In addition, the same study found that the microscopic orientations when comparing the fiber distribution before and after clearing were not affected by the clearing process. The clearing process, however, caused an almost isotropic shrinkage of about 20%, see also [12,32,33]. Hence, the shrinkage had also occurred along the sample thickness. Reducing the thickness can actually be beneficial in SHG imaging as it facilitates detailed imaging due to a better in-depth signaling.

The samples were imaged to a depth of $400 - 700\,\mu$m in the microscopy coordinate system. Image analysis based on Fourier transform is used to quantify the distribution of collagen fibers. The automated process ensures a high reproducibility, but there are some challenges with the process. The Fourier transform as-

sumes a periodic signal, so a window should be applied to the images before the Fourier transform. In the current study, a tapered cosine window is used to minimize the loss of information at the edges of each image (layer). In addition, the pixelated nature of images makes it difficult to completely segment the image with a wedge filter. Nevertheless, it has been shown that the wedge filter can extract the orientation of collagen fibers well, as in the study [12], which was also observed in the current study (Fig. 6). For each sample, acquisition layers with a $5\,\mu$m interval across the thickness were examined with SHG. For all samples except P3-MVAL, one family of collagen fibers was identified based on their collagen fiber distribution in each layer. Sample P3-MVAL showed two different fiber families (Fig. 5) and the more prominent fiber family was used for further analysis. For each layer l, the collagen fiber distribution was characterized by two parameters in the von Mises distribution, namely the mean fiber angle and the concentration parameter. It was found that the mean fiber angle varies over the tissue thickness. However, this variation was not as significant as in the study [11]. The authors documented fibers that were circumferentially oriented at a depth of $100\,\mu$m from the ventricle side compared to radially oriented fibers at a depth of $100\,\mu$m from the atrium side. In the present study, this finding was only obtained in one sample (P2-MVAL). Nevertheless, the mean fiber angle for all samples varies on average by $\pm 12^\circ$ over the entire thickness. Even the averaged mean angle does not always align with the circumferential direction. It depends heavily on the location of the acquisition, as it was derived from other imaging modalities such as pFSDI [8,35].

The concentration parameter also varied over the tissue thickness, on average ± 0.31, which is more significant than that of the mean fiber direction. The SHG-measured concentration parameter was 1.16 ± 0.32 for all samples except P2-MVAL. On average, the samples exhibited a higher anisotropy at a depth of $5 - 50\%$ and a higher collagen content at a depth of $25 - 75\%$. This depth can correlate to the collagen-rich fibrosa layer in MV (Fig. 7). The layer-specific investigation of MV leaflets showed that the fibrosa layer covers 60% of the MV thickness in porcine [36] and 75% in ovine [37]. Similar to the mean fiber direction, it was previously determined that the collagen fiber dispersion is regionally dependent [35]. A recent study on ovine tricuspid valve used SHG to quantify the collagen structure [17]. The authors found a comparable variation of the mean fiber orientation and the concentration parameters over the thickness in relation to the present study.

The constitutive model agrees well with the planar biaxial mechanical tests (average $r^2 = 0.94$). The low neoHookean parameters, average of $\mu = 2.22 \pm 1.48$ kPa, underline the importance of the contribution of the collagen fibers to the mechanical behavior of the leaflets. The compliant matrix material is consistent with recent studies on the mechanical properties of porcine MV leaflets [14,38,39]. This study confirms the assumption that the collagen fibers can be modeled with a representative single fiber family. This can have a significant impact on the tissue characterization of MV leaflets and the numerical modeling of the mitral valve apparatus.

It was also observed that the collagen fibers are not always aligned with the circumferential direction. The same finding is also observed in mechanical tests. Fig. 9 shows the Cauchy stress versus stretch curves for samples P3-MVAL and P6-MVAL. From Table 1 the mean fiber angle for the first sample is 32°, which resulted in a similar stiffness in the circumferential and radial directions. For the second sample, the mean fiber angle is 81°, which leads to a more compliant circumferential direction. This undermines the general assumption that the fibers are oriented in either the stiffer or the circumferential direction. Therefore, a robust method of measuring the mean fiber angle is essential for tissue modeling of MV leaflets.

Finally, it should be mentioning that elastin fibers are not taken into account in this study and that the anisotropy is mainly attributed to the collagen structure. Nevertheless, scanning electron microscopy shows radially aligned elastin fibers in the belly and a rectilinear pattern in the hinge and coaptation area of the aortic valve leaflets spongiosa [40]. A further study on the layer-specific investigation of MV leaflets also found radially oriented elastin fibers and circumferentially oriented wisp-like strands of elastin in the atrialis/spongiosa layer of MV leaflets [36]. However, the same study found that this layer is stiffer in the circumferential direction due to the presence of some collagen fibers. In addition, the collagen fibers are seen as the main load carrier and the elastin fibers mainly contribute to the stress-strain curve in the toe region, as shown schematically by Schoen and Levy [41]. Therefore, in the present study, only one family of fibers is assumed as representative collagen fibers for tissue modeling. Furthermore, our current study has shown that the anisotropy of the mechanical behavior of the tissue is mainly determined by the collagen structure, as discussed in the previous paragraph. Nevertheless, there is a significant interaction between collagen and other constituents, as shown for MV leaflets in [36]. This is also comparable with other studies on the aortic valve leaflets [40,42,43]. For example, the seperation of the layers in aortic valve leaflets showed less extensibility in the radial direction for a separated fibrosa layer than the intact leaflet, possibly as a result of collagen-elastin interactions [42,43]. Although the current tissue model attributes the anisotropy to collagen fibers, the interaction of collagen and other constituents in the ECM affects the material parameters, both the matrix and the fiber material parameters.

There are several limitations to the current study. First, the small field of view of SHG imaging (hundreds of microns) limits the examination and its extension to the tissue scale. The regional dependence of the collagen fiber orientation and dispersion also underlines this limitation. For example, the averaged mean fiber direction was measured from -70° to $+80^\circ$, due to the different investigation site on the MV leaflets (Fig. 6). Even so, the mechanical tests are performed within the fiducial markers with an approximate area of 2 mm $\times$2 mm, while the SHG detection is carried out in the center of these markers with an area of 0.46 mm $\times$0.46 mm, which is comparable to the area enclosed by the fiducial markers. Second, this was an *in vitro* study that neglected the effects of pre-strain and active smooth muscles on the distribution of collagen fibers. Recent studies have highlighted the contribution of pre-strain and active smooth muscles to the mechanical response of the mitral valve leaflets [44–46]. Both the pre-strain and the active tension of the smooth muscles can change the mean fiber orientation and dispersion. Third, an *ex vivo* experimental setup, similar to the study in, e.g., [47], may be required for the validation of the tissue modeling. Fourth, the water lens used in this study had a different refractive index ($n = 1.33$) than the BABB solution ($n = 1.56$). Although high quality images were recorded with this objective, the image quality could be improved by using a special lens suitable for immersion medium BABB. Finally, this study focused on porcine samples. In future work we plan to extend the protocol to human mitral valves in health and disease. It is particularly important to know how the collagen fibers are dispersed and oriented over their entire thickness in myxomatous degeneration. In addition, a mechanical characterization of degenerative MV is of great interest. This information, together with the structural data from SHG, can improve current tissue simulations of the MV apparatus. It will also provide a quantified study of how collagen fiber are disrupted in related diseases.

5. Conclusion

In this study, the collagen structure of MV leaflets was quantified through the entire thickness with high transmural resolution. In addition, planar biaxial mechanical tests were performed to characterize the mechanical behavior of the tissue. The mean fiber angle and collagen dispersion were found to vary across the thickness. Despite this variation, a single representative fiber family in a constitutive tissue model can adequately capture the mechanical behavior of the tissue. In addition, it was found that the tissue matrix is compliant and that the collagen plays the main load carrier. Interestingly, the collagen fibers were not always aligned with the circumferential direction, which was also observed in mechanical tests. The current study provides a thorough understanding of the collagen structure variation in MV leaflets and its effects on the mechanical properties and modeling of the tissue. In the end, we hope that the data set provided can pave the way for quantifying the disruption of collagen fibers in myxomatous MV leaflets.

Declaration of Competing Interest

The authors declare that they have no known competing financial interests or personal relationships that could have appeared to influence the work reported in this paper.

Acknowledgement

We acknowledge Dr. Stig Urheim (Haukeland University Hospital, Department of Heart Disease, Bergen, Norway) for insightful discussions on mitral valve disease. We also thank Kathrin Torseth (Department of Cancer Research and Molecular Medicine, Faculty of Medicine, NTNU, Trondheim, Norway) for her assistance with tissue fixation and dehydration, and Astrid Bjørkøy (Department of Physics, NTNU, Trondheim, Norway) for her useful discussions on second harmonic generation microscopy.

References

[1] M.S. Sacks, Y. Enomoto, J.R. Graybill, W.D. Merryman, A. Zeeshan, A.P. Yoganathan, R.J. Levy, R.C. Gorman, J.H. Gorman, In-vivo dynamic deformation of the mitral valve anterior leaflet, Annals of Thoracic Surgery 82 (2006) 1369–1377.
[2] D. Wiltz, C.A. Arevalos, L.R. Balaoing, A.A. Blancas, M.C. Sapp, X. Zhang, K.J. Grande-Allen, Extracellular Matrix Organization, Structure, and Function, in: E. Aikawa (Ed.), Calcific Aortic Valve Disease, IntechOpen, 2013, pp. 3–30.
[3] R.A. Levine, A.A. Hagége, D.P. Judge, M. Padala, J.P. Dal-Bianco, E. Aikawa, J. Beaudoin, J. Bischoff, N. Bouatia-Naji, P. Bruneval, J.T. Butcher, A. Carpentier, M. Chaput, A.H. Chester, C. Clusel, F.N. Delling, H.C. Dietz, C. Dina, R. Durst, L. Fernandez-Friera, M.D. Handschumacher, M.O. Jensen, X.P. Jeunemaitre, H.L. Marec, T.L. Tourneau, R.R. Markwald, J. Mérot, E. Messas, D.P. Milan, T. Neri, R.A. Norris, D. Peal, M. Perrocheau, V. Probst, M. Pucéat, N. Rosenthal, J. Solis, J.-J. Schott, E. Schwammenthal, S.A. Slaugenhaupt, J.-K. Song, M.H. Yacoub, Mitral valve disease-morphology and mechanisms, Nat. Rev. Cardiol. 12 (2015) 689–710.
[4] A. Carpentier, F. Filsoufi, D. Adams, Carpentier'Sreconstructive valve surgery, Saunders Elsevier, Philadelphia, 2010.
[5] W.G. Cole, D. Chan, A.J. Hickey, D.E. Wilcken, Collagen composition of normal and myxomatous human mitral heart valves, Biochem. J. 219 (1984) 451–460.
[6] K. Tamura, Y. Fukuda, M. Ishizaki, Y. Masuda, N. Yamanaka, V.J. Ferrans, Abnormalities in elastic fibers and other connective-tissue components of floppy mitral valve, Am. Heart J. 129 (1995) 1149–1158.
[7] B. Yang, J. Lesicko, M. Sharma, M. Hill, M.S. Sacks, J.W. Tunnell, Collagen Fiber Orientation Mapping with Top Layer Discrimination Using Polarized Light Spatial Frequency Domain Imaging delmMbox(pSFDI) on Native Heart Tissue, in: Biomedical Optics 2014, Optical Society of America, 2014, p. BM4B.5.
[8] S.V. Jett, L.T. Hudson, R. Baumwart, B.N. Bohnstedt, A. Mir, H.M. Burkhart, G.A. Holzapfel, Y. Wu, C.H. Lee, Integration of polarized spatial frequency domain imaging (pSFDI) with a biaxial mechanical testing system for quantification of load-dependent collagen architecture in soft collagenous tissues, Acta Biomater 102 (2020) 149–168.
[9] R.P. Cochran, K.S. Kunzelman, C.J. Chuong, M.S. Sacks, R.C. Eberhart, Nondestructive analysis of mitral valve collagen fiber orientation, ASAIO Transactions 37 (1991) 447–448.
[10] J. Liao, L. Yang, J.S. Grashow, M.S. Sacks, Molecular orientation of collagen in intact planar connective tissues under biaxial stretch, Acta Biomater 1 (2005) 45–54.
[11] C.A. Carruthers, B. Good, A. D'Amore, J. Liao, R. Amini, S.C. Watkins, M.S. Sacks, Alterations in the Microstructure of the Anterior Mitral Valve Leaflet under Physiological Stress, in: ASME 2012 Summer Bioengineering Conference, Parts A and B, American Society of Mechanical Engineers, 2012, pp. 227–228.
[12] A.J. Schriefl, H. Wolinski, P. Regitnig, S.D. Kohlwein, G.A. Holzapfel, An automated approach for three-dimensional quantification of fibrillar structures in optically cleared soft biological tissues, Journal of the Royal Society Interface 10 (2013) 20120760.
[13] G.A. Holzapfel, Collagen in Arterial Walls: Biomechanical Aspects, in: P. Fratzl (Ed.), Collagen. Structure and Mechanics, Springer-Verlag, Heidelberg, 2008, pp. 285–324.
[14] A. Pokutta-Paskaleva, F. Sulejmani, M. DelRocini, W. Sun, Comparative mechanical, morphological, and microstructural characterization of porcine mitral and tricuspid leaflets and chordae tendineae, Acta Biomater 85 (2019) 241–252.
[15] J. Liao, L. Yang, J.S. Grashow, M.S. Sacks, The relation between collagen fibril kinematics and mechanical properties in the mitral valve anterior leaflet, J Biomech Eng 129 (2007) 78–87.
[16] W. Zhang, S. Ayoub, J. Liao, M.S. Sacks, A meso-scale layer-specific structural constitutive model of the mitral heart valve leaflets, Acta Biomater 32 (2016) 238–255.
[17] W.D. Meador, M. Mathur, G.P. Sugerman, T. Jazwiec, M. Malinowski, M.R. Bersi, T.A. Timek, M.K. Rausch, A detailed mechanical and microstructural analysis of ovine tricuspid valve leaflets, Acta Biomater 102 (2020) 100–113.
[18] S.J. Crick, M.N. Sheppard, S.Y. Ho, L. Gebstein, R.H. Anderson, Anatomy of the pig heart: comparisons with normal human cardiac structure, J. Anat. 193 (1998) 105–119.
[19] G.A. Holzapfel, J.A. Niestrawska, R.W. Ogden, A.J. Reinisch, A.J. Schriefl, Modelling non-symmetric collagen fibre dispersion in arterial walls, Journal of the Royal Society Interface 12 (2015) 20150188.
[20] E. Fagerholt, T. Borvik, O.S. Hopperstad, Measuring discontinuous displacement fields in cracked specimens using digital image correlation with mesh adaptation and crack-path optimization, Opt Lasers Eng 51 (2013) 299–310.
[21] H.-U. Dodt, U. Leischner, A. Schierloh, N. Jährling, C.P. Mauch, K. Deininger, J.M. Deussing, M. Eder, W. Zieglgänsberger, K. Becker, Ultramicroscopy: three--dimensional visualization of neuronal networks in the whole mouse brain, Nat. Methods 4 (2007) 331–336.
[22] G. Sommer, A.J. Schriefl, M. Andrä, M. Sacherer, C. Viertler, H. Wolinski, G.A. Holzapfel, Biomechanical properties and microstructure of human ventricular myocardium, Acta Biomater 24 (2015) 172–192.
[23] G. Sommer, C. Benedikt, J.A. Niestrawska, G. Hohenberger, C. Viertler, P. Regitnig, T.U. Cohnert, G.A. Holzapfel, Mechanical response of human subclavian and iliac arteries to extension, inflation and torsion, Acta Biomater 75 (2018) 235–252.
[24] MATLAB version 9.10.0.1613233 (R2021a), The Mathworks, Inc., Natick, Massachusetts, 2021.
[25] P. Berens, Circstat: a MATLAB toolbox for circular statistics, J Stat Softw 31 (2009) 1–21.
[26] C. Raub, A. Putnam, B. Tromberg, S. George, Predicting bulk mechanical properties of cellularized collagen gels using multiphoton microscopy, Acta Biomater 6 (2010) 4657–4665.
[27] G.A. Holzapfel, Nonlinear solid mechanics. a continuum approach for engineering, John Wiley & Sons, Chichester, 2000.
[28] G.A. Holzapfel, R.W. Ogden, S. Sherifova, On fibre dispersion modelling of soft biological tissues: a review, Proceedings of the Royal Society A: Mathematical, Physical and Engineering Sciences 475 (2019) 20180736.
[29] M.S. Sacks, Biaxial mechanical evaluation of planar biological materials, J Elast 61 (2000) 199–246.
[30] W. Zhang, Y. Feng, C.-H. Lee, K.L. Billiar, S. Michael, A generalized method for the analysis of planar biaxial mechanical data using tethered testing configurations, J Biomech Eng 137 (2015) 0645011.
[31] D.S. Richardson, J.W. Lichtman, Clarifying tissue clearing, Cell 162 (2015) 246–257.
[32] K. Becker, N. Jährling, S. Saghafi, R. Weiler, H.U. Dodt, Chemical clearing and dehydration of GFP expressing mouse brains, PLoS ONE 7 (2012) e33916.
[33] M.T. Ke, S. Fujimoto, T. Imai, SeeDB: a simple and morphology-preserving optical clearing agent for neuronal circuit reconstruction, Nat. Neurosci. 16 (2013) 1154–1161.
[34] M.J. Turunen, H. Khayyeri, M. Guizar-Sicairos, H. Isaksson, Effects of tissue fixation and dehydration on tendon collagen nanostructure, J. Struct. Biol. 199 (2017) 209–215.
[35] W. Goth, S. Potter, A.C.B. Allen, J. Zoldan, M.S. Sacks, J.W. Tunnell, Non-destructive reflectance mapping of collagen fiber alignment in heart valve leaflets, Ann Biomed Eng 47 (2019) 1250–1264.
[36] K.E. Kramer, C.J. Ross, D.W. Laurence, A.R. Babu, Y. Wu, R.A. Towner, A. Mir, H.M. Burkhart, G.A. Holzapfel, C.H. Lee, An investigation of layer-specific tissue biomechanics of porcine atrioventricular valve anterior leaflets, Acta Biomater 96 (2019) 368–384.
[37] C.-H. Lee, C.A. Carruthers, S. Ayoub, R.C. Gorman, J.H. Gorman, M.S. Sacks, Quantification and simulation of layer-specific mitral valve interstitial cells deformation under physiological loading, J. Theor. Biol. 373 (2015) 26–39.
[38] S. Jett, D. Laurence, R. Kunkel, A.R. Babu, K. Kramer, R. Baumwart, R. Towner, Y. Wu, C.H. Lee, An investigation of the anisotropic mechanical properties and anatomical structure of porcine atrioventricular heart valves, J Mech Behav Biomed Mater 87 (2018) 155–171.

[39] A. Anssari-Benam, Y.T. Tseng, G.A. Holzapfel, A. Bucchi, Rate-dependency of the mechanical behaviour of semilunar heart valves under biaxial deformation, Acta Biomater 88 (2019) 120–130.
[40] H. Tseng, K. Grande-Allen, Elastic fibers in the aortic valve spongiosa: a fresh perspective on its structure and role in overall tissue function, Acta Biomater 7 (2011) 2101–2108.
[41] F.J. Schoen, R.J. Levy, Tissue heart valves: current challenges and future research perspectives, J. Biomed. Mater. Res. 47 (1999) 439–465.
[42] I. Vesely, R. Noseworthy, Micromechanics of the fibrosa and the ventricularis in aortic valve leaflets, J Biomech 25 (1992) 101–113.
[43] J.A. Stella, M.S. Sacks, On the biaxial mechanical properties of the layers of the aortic valve leaflet, J Biomech Eng 129 (2007) 757–766.
[44] I.S. Nordrum, B. Skallerud, Smooth muscle in the human mitral valve: extent and implications for dynamic modelling, APMIS 120 (2012) 484–494.
[45] M.K. Rausch, N. Famaey, T.O. Shultz, W. Bothe, D.C. Miller, E. Kuhl, Mechanics of the mitral valve: a critical review, an in vivo parameter identification, and the effect of prestrain, Biomech Model Mechanobiol 12 (2013) 1053–1071.
[46] V. Prot, B. Skallerud, Contributions of prestrains, hyperelasticity, and muscle fiber activation on mitral valve systolic performance, Int J Numer Method Biomed Eng 33 (2017) e2806.
[47] C.H. Bloodworth, E.L. Pierce, T.F. Easley, A. Drach, A.H. Khalighi, M. Toma, M.O. Jensen, M.S. Sacks, A.P. Yoganathan, Ex vivo methods for informing computational models of the mitral valve, Ann Biomed Eng 45 (2017) 496–507.